Density scaling laws for the structure of granular deposits

Daniel Rodríguez-Pérez,[*] Jose L. Castillo,[†] and J. Carlos Antoranz[‡]

Departamento de Fisica Matematica y de Fluidos, Facultad de Ciencias, UNED, Madrid, Spain
(Received 31 January 2007; revised manuscript received 21 March 2007; published 25 July 2007)

The structure of granular deposits growing by arriving particles is analyzed using three-dimensional on-lattice Monte Carlo modeling of convective-diffusive particle deposition. The deposit density profile $\rho(h)$ depends on the particle dynamics and becomes formed by three different regions: a denser near-wall region at the deposit bottom in contact with the original plain surface, a middle uniform region with constant mean density, and an open and lighter active-growth region at the deposit outer surface. Fitting expressions for $\rho(h)$ valid in each region are proposed, based on the known features of deposits formed in the two limiting cases: ballistic deposition and diffusion-limited deposition. Also, a composite expression for $\rho(h)$ fitting the density profile throughout the deposit is given. All these expressions are written in terms of a length scale $l(\text{Pe})$ dependent on the particle Péclet number, which provides the relative importance of the convective motion to the diffusive transport for the particle.

I. INTRODUCTION

Nonequilibrium interface growth models have been extensively studied during the last 30 years [1–3]. The need for controlling the structure of deposits in areas such as material synthesis from powders or colloidal suspensions [4,5], particle filter performance monitoring [6–8], deposits formed by combustion generated particles on the surfaces confining the flue gas stream [9], or sedimentary rock properties estimation [10] has motivated some of this fundamental research. Two of the most studied cases are ballistic deposition (BD) [4] and diffusion-limited aggregation (DLA) [11] and deposition (DLD) [12]. In the BD case, the interface is formed by depositing identical particles that move following straight-line trajectories. This would be the case of aerosol particles inertially impinging onto a duct wall [13] or calcite particles sedimenting to form a limestone rock [10,14]. In the DLD case, the deposit is formed by attaching particles which arrive following purely Brownian paths. From the point of view of the growing deposit geometry, these two limiting growth models lead to prototypes of self-affine fractals [16,17] and self-similar fractals [12,15], BD and DLD, respectively. The deposit morphology is thus related to the particle dynamical behavior near the surface. Therefore, it is worthwhile to simulate deposits formed by different particle arrival mechanisms to obtain the bulk deposit properties (density) and surface features (roughness) as a function of the parameters that control the particle dynamics. The microstructure of these heterogeneous deposits determines the material macroscopic properties [18,19] such as strength, permeability, effective thermal conductivity, diffusivity for vapor molecules, reactivity for labile molecules, etc.

The DLD model is valid for particles moving in a stochastic manner due to thermal fluctuations. On the other hand, the BD model applies to particles moving in a deterministic way (due to either inertia, sedimentation, or phoretic forces driving the particles toward the collecting surface). However, in general, the particle motion is neither purely stochastic nor completely deterministic. Rather, the particle motion can be split into two contributions: a mean velocity V and a Brownian motion with a diffusion coefficient $\mathcal{D}$. The particle mean velocity can be adjusted by controlling the intensity of the driving mechanism (gravitational sedimentation, inertia, thermal gradient, electric field). Thus, the arrival velocity of particles to the surfaces confining particle laden gas flows due to particle inertia can be varied by adjusting the particle Stokes number [20] by means of changes in the gas flow field, in the surface orientation with respect to the mainstream, or in the surface curvature [21,22]. Also, the strength of particle thermophoresis (drift of particles toward the cooler regions under the presence of strong temperature gradients) depends on the imposed temperature difference between the mainstream gas and the surface [23], and the intensity of particle photophoresis (particle drift in a radiative field induced by slip due to the inhomogeneous temperatures induced by the absorption of radiation) can be controlled by the intensity of the radiative field [24]. Changes in the deposit structure (and thus in its physical and chemical properties) induced by modulating the phoretic force have been experimentally reported [8,25,26] (although these works were not intended to obtain a detailed characterization of the synthesized material deposits and do not provide the data required to compare with theoretical estimations). The particle convective-diffusive motion is characterized by the relative intensity of the convective (deterministic) contribution to the diffusive (stochastic) part—that is, by the particle Péclet number [7,27] $\text{Pe}=Va/\mathcal{D}$, where a stands for the characteristic length (the particle diameter here).

In general, deposits formed by particles arriving to an initially flat wall become structured in three levels: a denser near-wall (NW) region, a uniform region with constant mean density, and an open and lighter active-growth (AG) region [7]. The NW region comes from the early deposition stages of the particle attaching on the initial clean surface which is not shadowed by any formed deposit structure, rendering a high-density layer. The uniform region corresponds to the

*daniel@dfmf.uned.es
†jcastillo@ccia.uned.es
‡jcantoranz@dfmf.uned.es

steady growth of the deposit with constant mean density. Both the NW region and the uniform region are frozen regions because no new particles arrive there. The AG region is the topmost layer of the deposit where particles are still becoming attached. Here, the density is smaller and vanishes with increasing height.

Studies of aggregates being formed by particles [28–30] have shown that the change from diffusive to deterministic particle motion induces a crossover from a fractal structure to a compact aggregate. Large aggregates are fractals up to a length scale of the order of $\mathcal{D}/V$; that is, they can be considered as pseudohomogeneous bodies with fractal structure on the small scale. For particle deposits this crossover also exists [31] and determines the average deposit density in the uniform region. Characterizing the density as the solid fraction, the mean density in this uniform region is well described by the expression

$$\bar{\rho}(\mathrm{Pe}) = \rho_\infty (1 + \mathrm{Pe}_0/\mathrm{Pe})^{-D}, \tag{1}$$

where $D \simeq 0.52$, ρ_∞ is the ballistic deposit average density ($\rho_\infty \simeq 0.302$ for on-lattice simulations with "cubic particles," as reported in this work, which is higher than $\rho_\infty \simeq 0.18$ found for off-lattice simulations with spherical particles), and Pe_0 is the crossover Péclet number ($\mathrm{Pe}_0 = 4.8$ for on-lattice simulations). This expression suggests a local fractal structure up to a length scale [31]

$$l(\mathrm{Pe}) = (1 + \mathrm{Pe}_0/\mathrm{Pe})a. \tag{2}$$

This result is in agreement with the value of the exponent $D = 3 - D_{DLA}$, where $D_{DLA} = 2.48$ is the fractal dimension of a DLA fractal in three-dimensional (3D) simulations [15].

A recent result by Ferreira *et al.* [30] provides some further insight into this fractal-compact crossover for aggregates. These authors suggest an asymptotic numerical fitting expression for $l(\mathrm{Pe})$, somewhat different from ours, but compatible with it in the realm of 2D simulations (except for the orientation dependence induced by the *anisotropic diffusion* taken in [30]). The box-counting density expression in [30] corresponds to that of a fat fractal. This result is compatible with the existence of an average density (1) and the box-counting results presented in [31].

In the limit of ballistic deposition, the interface will belong to the Kardar-Parisi-Zhang (KPZ) universality class [17]. Although some recent results disagree with this classification [32,33], we will identify BD as belonging to the KPZ universality, because KPZ is the continuous dynamical growth model which leads to values of the dynamical exponents closest to BD. For the deposit interface, a crossover from a KPZ-like self-affine interface [16,17] to a DLA-like self-similar interface [12] is expected when the Pe number decreases and tends to zero. When an appropriate definition of the interface is taken [31] (weighting the active site heights with their attachment probabilities), the interface is shown to become KPZ-like after an initial transient (corresponding to the early stages of DLA trees growth). The interface weighting leads to a dynamical definition of the interface, which can also be linked to the density profile evolution, as will be used below.

The aim of this work is to obtain the laws for the density profile in the granular material in terms of the (grain) particle Péclet number. These laws capture the previously cited scaling features and show the different deposit structures as the particle dynamics changes from a convective motion (high Péclet number) to a diffusive transport regime (low Péclet number).

II. MODELS AND METHODS

Deposits are formed by convective-diffusive arrival of particles. The particle motion is simulated by the 3D on-lattice Monte Carlo algorithm already introduced elsewhere [31] (adapted from [7,27]). The space is divided into cubic cells of side a, the characteristic lattice length as well as the particle diameter. Each cubic cell can have three labels: empty, occupied, or active. Active cells are those that can become occupied by a new arriving particle. The attachment of a new particle changes the cell label from active to occupied and also activates the neighbor empty cells. Initially, the cells at the bottom of the simulation domain (representing the deposition wall) are labeled active, and empty otherwise. In the 3D simulation domain, horizontal periodic boundary conditions are assumed, with a spatial periodicity equal to the lateral extension of the domain.

To ensure an isotropic diffusivity, each Monte Carlo time step consists of two stages: a deterministic stage where the particle moves vertically one cell toward the wall and a random stage formed by several random walk jumps (from the current cell to any of the six neighbor cells) with a Péclet-number-dependent probability (see Ref. [31] for details). This election allows the simulation of any value of the Péclet number with *isotropic diffusion*. The motion of a particle ends when it arrives to an active cell; there, the particle attaches to the active cell and causes the deposit growth.

An alternative way to simulate this type of motion, usually found in the literature, is by means of a biased Brownian motion [30,34]—that is, a change in the diffusion probabilities dependent on the direction of the motion. However, as was demonstrated in [31], this model, restricted to a lattice, does not reproduce the average properties of a convective-diffusive motion and causes an unrealistic anisotropic diffusion.

In the simulated deposits, the density profile $\rho(h)$ is measured as a solid fraction (fraction of occupied cells at a given height h). We locate the initially clean deposition wall at $h = 0$ and the first particle level at height $h = a$. The maximum deposit height h_{max}, the upper limit of the AG region, is the height of the topmost active site of the deposit. Pe values ranged from 0.01 (mainly diffusive particle motion) to 1000 (mainly ballistic particle trajectories). Deposits were grown in a lattice with $L = 400a$ as base side length and up to $h = 800a$ in height. All the results are averages over 10 different simulations for each Pe.

III. RESULTS AND DISCUSSION

The structure of the uniform region was already characterized by a constant mean density, Eq. (1) [31]. In the fol-
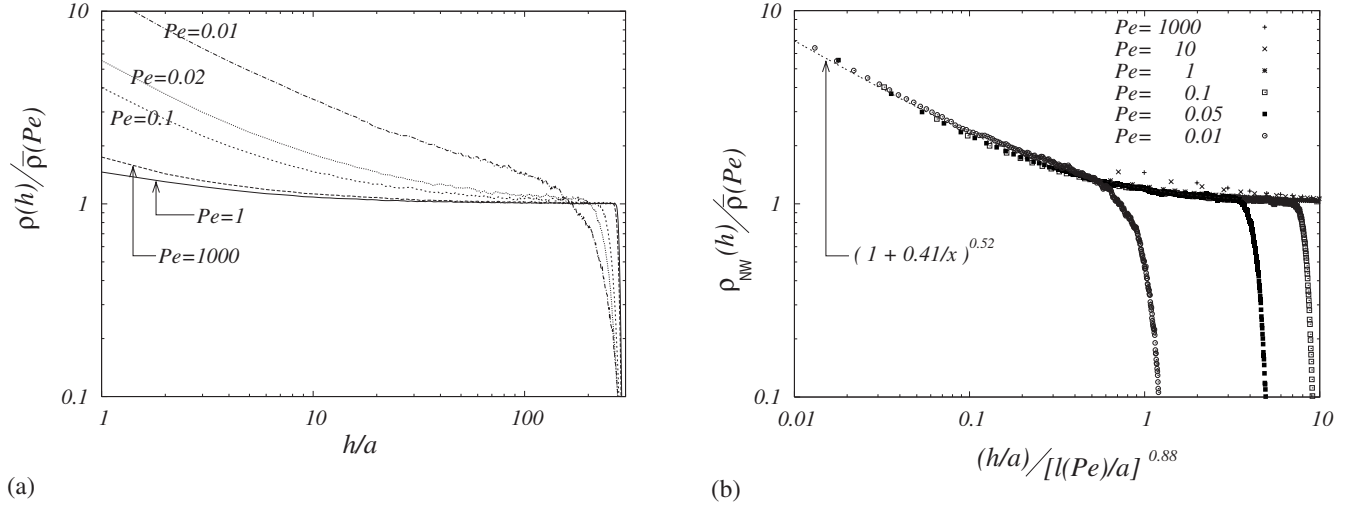
(a)

(b)

FIG. 1. Log-log density profiles (with $h_{max}=300a$) normalized to the uniform region density $\bar{\rho}(Pe)$: (a) versus the deposit height and (b) collapsed according to Eq. (3).

lowing, we will focus on the NW region and on the AG region density profiles.

A. Near-wall region

Figure 1(a) depicts the averaged density profiles for several values of the particle Péclet number. The log-log scale emphasizes the denser NW regions. These plots suggests a power-law behavior near the wall (as is the DLD case [12]). Figure 1(b) shows the fitting of the NW density profiles $\rho_{NW}(h,Pe)$, given by

$$\rho_{NW}(h,Pe) = \bar{\rho}(Pe)\xi_{NW}(h,Pe), \qquad (3)$$

where

$$\xi_{NW}(h,Pe) \equiv \left(\frac{h}{h + A[l(Pe)/a]^{D_1}}\right)^{-D}$$

and $l(Pe)$ is the crossover length in Eq. (2), $A \simeq 0.41a$, $D_1 \simeq 0.88$, and $D=0.52$ [as in Eq. (1)].

An important property of the deposit is the characteristic length $l(Pe)$ given by Eq. (2). As was explained before, it plays the role of a decorrelation length for the local fractal behavior. However, Eq. (3) suggests that it is also a relevant quantity in the whole frozen region. Equation (3) should render a generalization of the self-similar density profile of a fractal diffusion limited deposit in the limit $Pe \rightarrow 0$ (purely diffusive particles) given by [1]

$$\rho_{DLD}(h) \sim h^{D_{DLA}-3}.$$

Indeed, this expression is in good agreement with the limit $Pe \rightarrow 0$ of Eq. (3).

The data fitting of the NW region (3) is not very good for $Pe > 1$. In this limit, the NW region is too thin because the uniform region density is achieved after just a few particle heights. For example, for $Pe=10$, a straightforward calculation shows that only some ten particle levels are reliable for fitting. Also the deposition of the first particles arriving to a

clean surface is purely random, because there are not enough deposited particles to interact with [35]. This hardly occurs for $Pe < 1$, because the large volume explored by a random walker before deposition improves early particle-deposit interaction.

B. Active-growth region

On the other hand, Fig. 2(a) shows the AG region density profiles for several Péclet numbers. Referring the deposit heights to h_{max}, the log-log plot in Fig. 2(b) suggests a power law behavior $\rho_{AG}(h,Pe)$ within that region:

$$\rho_{AG}(h,Pe) \propto (h_{max}-h)^{\gamma}. \qquad (4)$$

The time evolution of the AG region is expected to be always ruled by the dynamical scaling of a KPZ interface. Thus, for a given Péclet number, the arrival heights should be distributed inside the interface width following the KPZ scaling—that is, as $\sim t^{\beta}$ (where β is the dynamic scaling exponent) [31]. However, looking the interface as a front advancing with constant velocity, this scaling can also be written as $\sim \bar{h}^{\beta}$, where $\bar{h}$ is the deposit mean height. Indeed, as is shown in Fig. 2(b), the scaling of the depth to h^{β} collapses the time evolution of the AG region profile onto a single curve:

$$\rho_{AG}(h,Pe) \propto \left[\frac{(h_{max}-h)/a}{(h/a)^{\beta}}\right]^{\gamma}, \qquad (5)$$

where γ depends on Pe in a nontrivial way, but remains almost constant during the whole deposit growth history. h_{max} increases linearly with time, providing a Pe-dependent deposit growth velocity. Equation (5) applies even during the early deposition stages, when there is no uniform region yet [see Fig. 2(b) for $Pe=0.05$].

The characteristic length scale in the AG region (for Pe > 0) is the interface width $w \sim t^{\beta} \sim \bar{h}^{\beta}$. The exponent γ in (5) depends on Pe varying monotonically from $\gamma \simeq 1.5$ (for Pe
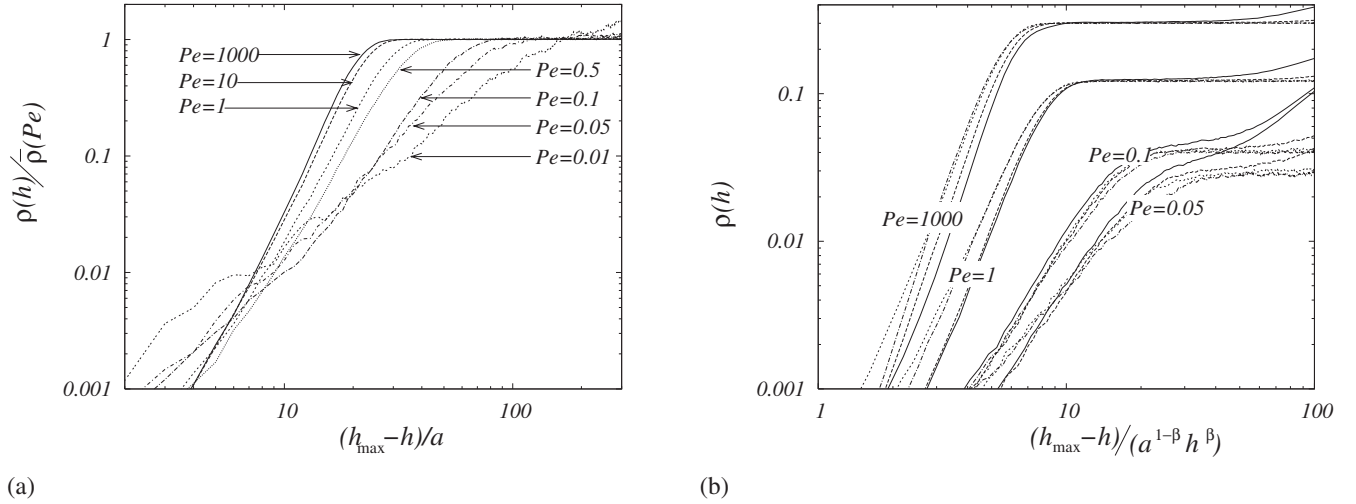
FIG. 2. Log-log density profiles in the AG region. (a) Normalized density, versus depth for $h_{max}=400a$. (b) Density profiles for different Pe and values of $h_{max}=100a$ (solid line), $200a$ (dashed line), $400a$ (dotted line), and $800a$ (dash-dotted line).

=0.01) to $\gamma \simeq 4$ (for Pe=1000). In the DLD limit, according to simple scaling arguments, a value $\gamma = D_{DLA} - 1$ is expected, validating our numerical value of γ in the low-Péclet-number limit. In the opposite limit (Pe→∞), a value $\gamma \simeq 4$ is obtained for purely BD simulations, although to the best of our knowledge this particular value is not supported by any theoretical argument. The fitting of the AG region (5) is worse in the limit of Pe≤0.1 and for long times. This is due to the interface saturation caused by the imposed (finite) horizontal periodicity of the simulation lattice, an effect already discussed [31], in terms of the deposit characteristic length l relative to the simulation box size L. Saturation makes no longer valid the dynamical roughening law $w \sim \bar{h}^{\beta}$. The failure to collapse the Pe≥1 simulations to one single curve, as shown in Fig. 2(b), seems to be due to the small scale used in the abscissa region (the distance between the curves is less than one unit in the horizontal axis) and probably also due to the small sample size employed in this study.

As in the case of Eq. (3), Eq. (5) can be extended to match with the uniform region density far from h_{max}. This can be accomplished by defining

$$\rho_{AG}(h,Pe) = \bar{\rho}(Pe)\xi_{AG}(h,Pe), \qquad (6)$$

where

$$\xi_{AG}(h,Pe) \equiv \frac{\rho_0 \left[\dfrac{(h_{max}-h)/a}{(h/a)^{\beta}} \right]^{\gamma}}{\sqrt{\rho_p^2 + \rho_0^2 \left[\dfrac{(h_{max}-h)/a}{(h/a)^{\beta}} \right]^{2\gamma}}}.$$

The coefficient $\rho_p \equiv 1$ corresponds to the particle density, whereas ρ_0 depends on Pe and varies in the range from 5×10^{-4} (for Pe=1000) to 5×10^{-2} (for Pe=0.01). Figure 3 shows the good fitting of the density profile to this expression in the upper part of the deposit. The fitting is good even for Pe=0.05 and for deposit heights as high as $400a$. Above that height, the saturation effects begin to be important be-

cause the fractal trees and the lattice lateral size become of the same length scale.

Equations (3) and (6) suggest a composite fitting formula for the density profile throughout the deposit in the form

$$\rho(h,Pe) = \bar{\rho}(Pe)\xi_{NW}(h,Pe)\xi_{AG}(h,Pe), \qquad (7)$$

which includes in a single expression the behavior in each deposit region. This is an appealing simple expression that shows a good behavior even in those cases where the sectional expressions (3) and (5) fail (for instance, in the absence of an uniform region, pointed out by arrows in Fig. 3).

IV. CONCLUSIONS

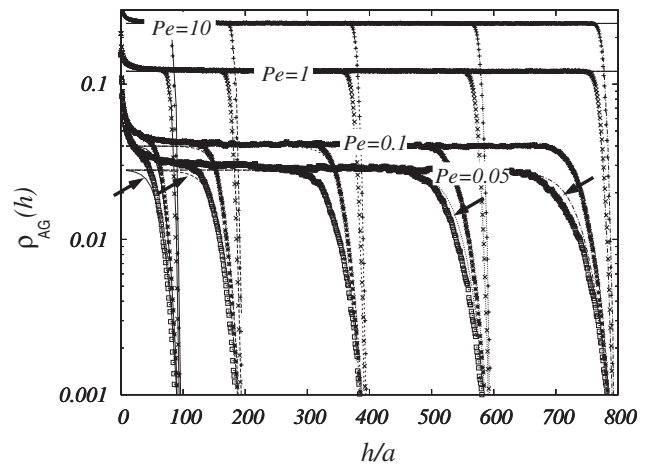Equation (7) summarizes the results in the three distinguishable deposit layers, providing a single fitting formula

FIG. 3. Density profile fitting according to Eq. (6) for Pe=10 (plus signs), 1 (crosses), 0.1 (stars), and 0.05 (open squares) and $h_{max}=100a, 200a, 400a, 600a, 800a$. The arrows show the locations where the sectional fits fail due to the lack of uniform region (left) or due to finite-size effects (right).

for the granular deposit formed by the convective-diffusive arrival of particles. This result may be useful to control the density of a heterogeneous material synthesized from powders by adjusting the intensity of the driving force that pushes the particles toward the deposit (for instance, controlling the particle inertia by adjusting the surface orientation or curvature [21,22], thermophoresis by adjusting the temperature difference between the deposit and the mainstream [23], or photophoresis by imposing a radiative field [24]). Also, from the experimentally measurable density profiles, Eq. (7) can be used to measure the effectivity (or intensity) of the mechanism which drives the particle mean motion.

Previous results focused on the average bulk structure (mean density or, equivalently, mean deposit height) and on the asymptotic values of the interface properties (mainly width and, in general, roughening universality class) [31]. This work complements [31], giving the density profile for an arbitrary time (up to the interface saturation in our simulations) and for arbitrary heights. Both the near-wall region [Eq. (3)] and the active-growth region [Eq. (5)] are well fitted to a convective-diffusive model that shows the crossover

from a diffusion-limited behavior to a compact-ballistic regime.

The proposed fitting formula (7) matches the density profile of the near-wall and active-growth regions through the uniform region. The functional form depends on some coefficients that vary nontrivially with the Péclet number. Equation (7) brings together some basic features of ballistic and diffusion-limited deposits, but further analyses are needed to explain the values of these coefficients.

[1] T. Vicsek, *Fractal Growth Phenomena* (World Scientific, Singapore, 1989).

[2] A. L. Barabási and H. E. Stanley, *Fractal Concepts in Surface Growth* (Cambridge University Press, Cambridge, England, 1995).

[3] P. Meakin, *Fractals, Scaling and Growth far from Equilibrium* (Cambridge University Press, Cambridge, England, 1998).

[4] M. J. Vold, J. Colloid Sci. **14**, 168 (1959).

[5] M. J. Vold, J. Colloid Sci. **18**, 684 (1963).

[6] P. Meakin, Phys. Rev. A **27**, 2616 (1983).

[7] D. Houi and R. Lenormand, in *Kinetics of Aggregation and Gelation*, edited by F. Family and D. P. Landau (Elsevier, New York, 1984), pp. 173–176.

[8] A. G. Konstandopoulos, E. Skaperdas, and M. Masoudi, SAE Trans. **111**, 434 (2002).

[9] D. E. Rosner, A. G. Konstandopoulos, M. Tassopoulos, and D. W. Mackowski, in *Inorganic Transformations and Ash Deposition During Combustion*, edited by S. A. Benson (ASME, New York, 1992), pp. 585–606.

[10] R. Dasgupta, S. Roy, and S. Tarafdar, Physica A **275**, 22 (2000).

[11] T. A. Witten and L. M. Sander, Phys. Rev. Lett. **47**, 1400 (1981).

[12] Z. Rácz and T. Vicsek, Phys. Rev. Lett. **51**, 2382 (1983).

[13] A. G. Konstandopoulos, Powder Technol. **109**, 262 (2000).

[14] S. Tarafdar and S. Roy, Physica B **254**, 28 (1998).

[15] S. Tolman and P. Meakin, Phys. Rev. A **40**, 428 (1989).

[16] P. Meakin, P. Ramanlal, L. M. Sander, and R. C. Ball, Phys. Rev. A **34**, 5091 (1986).

[17] M. Kardar, G. Parisi, and Y.-Ch. Zhang, Phys. Rev. Lett. **56**, 889 (1986).

[18] M. Tassopoulos and D. E. Rosner, AIChE J. **38**, 15 (1992).

[19] S. Torquato, *Random Heterogeneous Materials: Microstructure and Macroscopic Properties* (Springer-Verlag, Berlin, 2002).

[20] J. L. Castillo, J. Macias, and P. L. Garcia-Ybarra, J. Aerosol Sci. **28**, S733 (1997).

[21] A. G. Konstandopoulos and D. E. Rosner, Int. J. Heat Mass Transfer **38**, 2305 (1995).

[22] A. G. Konstandopoulos and D. E. Rosner, Int. J. Heat Mass Transfer **38**, 2317 (1995).

[23] P. L. García-Ybarra and J. L. Castillo, J. Fluid Mech. **336**, 379 (1997).

[24] J. L. Castillo, D. Mackowski, and D. E. Rosner, Prog. Energy Combust. Sci. **16**, 253 (2000).

[25] M. Tatlier, Fractals **11**, 77 (2003).

[26] Y. Yu, J. L. Shui, S. Xie, and C. H. Chen, J. Aerosol Sci. **39**, 276 (2005).

[27] M. Tassopoulos, J. A. O'Brien, and D. E. Rosner, AIChE J. **35**, 967 (1989).

[28] P. Meakin, Phys. Rev. B **28**, 5221 (1983).

[29] T. Nagatani, Phys. Rev. A **39**, 438 (1989).

[30] S. C. Ferreira, S. G. Alves, A. Faissal Brito, and J. G. Moreira, Phys. Rev. E **71**, 051402 (2005).

[31] D. Rodríguez-Pérez, J. L. Castillo, and J. C. Antoranz, Phys. Rev. E **72**, 021403 (2005).

[32] T. Nagatani, Phys. Rev. E **58**, 700 (1998).

[33] E. Katzav and M. Schwartz, Phys. Rev. E **70**, 061608 (2004).

[34] M. Castro, R. Cuerno, A. Sánchez, and F. Domínguez-Adame, Phys. Rev. E **62**, 161 (2000).

[35] F. D. A. Aarao Reis, Phys. Rev. E **73**, 021605 (2006).